LA-UR- 08-4808

Approved for public release; distribution is unlimited.

Title:	Theoretical Analysis of Subzero Start-Up for Polymer Electrolyte Fuel Cells
Author(s):	Jixin Chen Yun Wang Partha P. Mukherjee
Intended for:	Paper for the PEM Fuel Cells Proceedings, PRIME, 214th Electrochemical Society Meeting, Honolulu, HI, October 12-17, 2008

Los Alamos
NATIONAL LABORATORY
EST. 1943

Form 836 (7/06)

Theoretical Analysis of Subzero Start-Up for Polymer Electrolyte Fuel Cells

Jixin Chen[a], Yun Wang[a], and Partha P. Mukherjee[b]
[a]Renewable Energy Resources Lab and National Fuel Cell Research Center, The University of California, Irvine, California, 92697-3975, USA
[b]Los Alamos National Laboratory, Los Alamos, NM, 87545, USA

Abstract

This paper investigates interaction of the electrochemical kinetics, oxygen transport and solid water formation within polymer electrolyte fuel cell (PEFC) electrode during cold start. Followed by the analysis of Wang [1], we simplify the one-dimensional model of electrode processes, which allows solving the profiles of important quantities and directly relating the ice impact mechanisms to surface overpotential. The key parameters that govern these profiles are evaluated in the range of the relevant factors for a typical fuel cell. We also decouple the mechanisms of solid water impacts and compare their importance. This study is valuable for studying the characteristics of cold-start for PEFCs.

INTRODUCTION

The polymer electrolyte fuel cell (PEFC) has been regarded as a potential power source for various applications due to its significant advantages, i.e. high efficiency, low emission, silence and simplicity [2]. While most of the efforts focus on the steady-state operation of fuel cells, their dynamic behaviors lack thorough investigation although the paramount importance has been gradually realized. PEFC will frequently encounter transient operation in practice, e.g. startup of automotive PEFCs. Identification of the physics governing PEFC transient is the key to ultimate advancement of fuel cell dynamic characteristics. Dynamic modeling has been attempted by several groups. One of the earliest dynamic models was developed by Amphlett et al. [3], which predicted evolutions of the cell voltage, power and stack temperature upon perturbations. Wang and Wang [4] [5] developed a 3-D dynamic model considering the major transient processes in PEFC including gas transport, membrane hydration and double-layer discharge. Overshoot/undershoot behaviors were observed during step changes under varying operating conditions. In their experimental work, Yan et al. [6] conducted studies on the dynamic behavior of PEFC under a series of changing operating parameters. Chen and Zhou [7] investigated the startup characteristics and dynamic behaviors of a PEFC stack and investigated channel pressure drop. Further, automobile PEFCs must be able to start up in a subzero environment, which adds additional process of water phase change to the dynamic behaviors. Under such condition, produced water may freeze instantaneously at the reaction sites, covering and hence reducing the electrochemical active surfaces in the catalyst layer (CL) and plugging the open pores in the gas diffusion layer (GDL). Exploring the mechanism of heat/mass transfer and electrochemical kinetics during PEFC cold start are still ongoing research [8] [9] [1] [10]. Following previous work by Wang [1], in this paper we further explores the electrochemical kinetics and transport phenomena in PEFC electrodes during cold start. The major physical and operating parameters as well as dimensionless constants that govern the profiles of major quantities during cold start are discussed and analyzed in detail. The results will improve the understanding of the electrochemical and transport physics during PEFC cold start.

MODELING APPROACH

Figure 1 schematically shows the components of a PEFC and details of cathode electrode. Following the analysis approach outlined in Ref. [1], the cold-start model can be established as shown below:

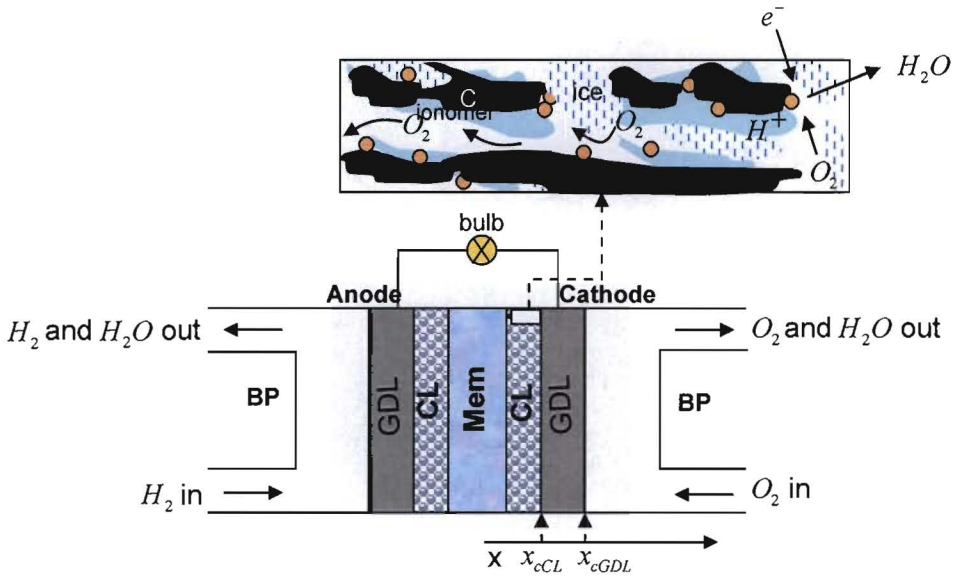

Fig. 1. Schematics of a PEFC and cathode electrode during cold start.

During cold start, solid water may form due to water production at subzero temperature. The solid water mostly stays in the local electrode due to lack of mechanisms to transport and typically attach on the surface of the solid matrix of the composite electrode. The electrochemical active surface in the catalyst layer may be reduced due to solid water presence. Similar to modeling of liquid water, this impact can be accounted for by modifying the Butler–Volmer equation, where a term related to ice volume fraction s_{ice} is added. After approximated by the Tafel kinetics due to the sluggish kinetics of oxygen reduction reaction (ORR), the reaction rate can be expressed by:

$$j_c = -a_0 i_{0,T}^c (1 - s_{ice})^{\tau_a} \frac{C^{O2}}{C^{O2,ref}} \exp\left(-\frac{\alpha_c F}{RT} \cdot \eta\right) \tag{1}$$

In Eq. (1), α_c, the cathode transfer coefficient, depends on temperature [11] [12]. In a Pt/Nafion interface, for example, $d\alpha/dT = 2.3\times10^{-3}$ [11]. α_c may vary from 0.5 to 1.0. In particular, α_c of 1 is frequently used in PEFC modeling and analysis [13][14], although 0.5 is adopted in some studies [15] [16].

The surface overpotential is defined as

$$\eta = \Phi_s - \Phi_e - U_o \tag{2}$$

Φ_s and Φ_e are electronic and electrolyte phase potentials, respectively. Typically due to the high electronic conductivity, Φ_e remains constant in the cathode. Φ_s usually varies

spatially due to the ionic resistance. The equilibrium potential, U_o, is a function of temperature:

$$U_o = 1.23 - 0.9 \times 10^{-3}(T - 298) \tag{3}$$

Temperature also affects the ORR kinetics, which can be expressed in the Arrhenius form:

$$i_{0,T}^c = i_0^c \exp\left[-\frac{E_a}{R}\left(\frac{1}{T} - \frac{1}{353.15}\right)\right] \tag{4}$$

Where E_a denotes the activation energy for ORR at the Pt/Nafion electrode [11].

In addition, solid water will narrow the diffusion passages of oxygen and hamper its transport to the reaction site. A general oxygen transport equation in one dimension can be expressed as:

$$\frac{\partial \varepsilon C^{O2}}{\partial t} + \frac{\partial u C^{O2}}{\partial x} = \frac{\partial}{\partial x}\left[D^{O2,eff}\frac{\partial C^{O2}}{\partial x}\right] + S^{O2} \tag{5}$$

Two types of diffusive transport are considered here. One is the molecular diffusion, which takes place when the mean free length of molecules is relatively large compared with the pore size. In GDLs, molecular diffusion dominates and its diffusion coefficient is related to temperature and pressure:

$$D_M^{O2} = D_{M,0}^{O2}\left(\frac{T}{353}\right)^{3/2}\left(\frac{1}{P}\right) \tag{6}$$

The other is the Knudsen diffusion, which occurs in situations in which gas molecules collide more frequently with pore walls than with other gas molecules. This type of diffusion is encountered when the mean free path of gas molecules is of the order of the pore characteristic length scale, which occurs in the catalyst layer. The Knudsen diffusion coefficient is around $2.64 \times 10^{-5} m^2/s$ [1] in the PEFC catalyst layer. To combine the two mechanisms in the catalyst layer, the harmonic mean is taken to calculate the average diffusivity. For analysis proposes, we denote the average diffusion coefficient in the catalyst layer as $D_K^{O_2}$ to distinguish from the one in GDLs where the molecular diffusion dominates. To account for the porosity and tortuosity factor, τ, of a porous media, the effective gas diffusion coefficient is given by

$$D^{O2,eff} = \frac{\varepsilon}{\tau} D^{O2} = \varepsilon^{\tau_{d,0}} D^{O2} \tag{7}$$

where the Bruggeman factor, $\tau_{d,0}$, is constant, indicative of tortuosity of a porous medium. Note that $\tau_{d,0}$ may vary, depending on the structure of the porous media. Typically 1.5 is used for this parameter [16] [17]. A direct numerical simulation of electrochemsitry coupled species and charge transport on a representative reconstructed CL structure based on actual 2D CL micrographs, shown in Fig. 2, suggests a value of $\tau_{d,0} \sim 4.0$ and takes into account the microstructural tortuosity effect on the underlying transport [18].

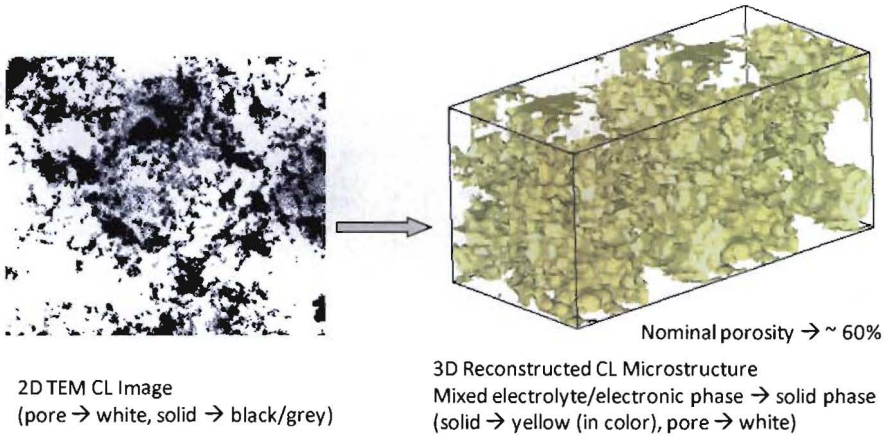

Fig. 2. 3D reconstructed CL microstructure using a stochastic reconstruction method [18].

As mentioned previously, solid water attaches on the surface of the wall, narrowing the diffusion passages. To account for this effect, again we follow the approach in liquid-water transport:

$$D^{O2,eff} = [\varepsilon(1 - s_{ice})]^{\tau_d} D^{O2} \tag{8}$$

It was found that the porosity ε of GDL may vary from 0.6 to 0.8, depending on the compression over it [19] [20]. Pasaogullari et al. [21] used 0.75 in their study. Furthermore, in Lin et al.'s study of optimization of key parameters in PEFCs, ε of GDL was set 0.5 [22]. In addition, they also adopted a very wide range of porosity of the catalyst layer, which varies from 0.3 to 0.8.

The drop of oxygen concentration across the GDL can be estimated by only considering the diffusive transport:

$$\Delta C^{O2}_{cGDL} = C^{O2}_{cGDL} - C^{O2}_{cCL} = \frac{I}{4F} \frac{\delta_{GDL}}{D^{O2,eff}_{M} \varepsilon^{\tau_{d,0}}_{GDL}} \tag{9}$$

It should be noted that different materials have been used for GDLs, e.g. carbon paper and carbon cloth are the major options [17] [23]. Also GDL thickness may vary from 100 to 350 micro meters. For example, in Nitta et al.'s experimental study on GDL inhomogeneous compression [24], GDL thickness varies from 150 to 350 μm.

In the catalyst layer, assuming diffusion is the dominant transport mechanism and reaction rate is uniform, the oxygen profile can be obtained (see Figure 1 for x_{cCL}) [1]:

$$\frac{C^{O2}}{C^{O2}_{cCL}} = 1 - \frac{I}{8F}\frac{\delta_{CL}^2 - (x - x_{cCL} + \delta_{CL})^2}{C^{O2}_{cCL}\delta_{CL}D_K^{O2}[\varepsilon_{CL}(1-s_{ice})]^{\tau_d}} = \left[1 - Da\frac{1-(\frac{x-x_{cCL}}{\delta_{CL}}+1)^2}{\varepsilon_{CL}^{\tau_d-\tau_{d,0}}[(1-s_{ice})]^{\tau_d}}\right] \quad (10)$$

where the dimensionless parameter, Da, is called the Damköhler number defined as

$$Da = \frac{I}{8F}\frac{\delta_{CL}}{C^{O2}_{cCL}D_K^{O2}\varepsilon_{CL}^{\tau_{d,0}}} = \frac{\text{Reaction rate}}{\text{Mass transport rate}} \quad (11)$$

Note that several key parameters, such as operating pressure, current density, and catalyst layer thickness, are lumped in Da. In addition, it also reflects the GDL impact through the value of C^{O2}_{cCL}. Combining Eqs. (9) and (11) yields:

$$Da = \frac{I}{8F}\frac{\delta_{CL}}{D_K^{O2}\varepsilon_{CL}^{\tau_{d,0}}}\frac{1}{C^{O2}_{cGDL} - \frac{I}{4F}\frac{\delta_{GDL}}{D_M^{O2,eff}\varepsilon_{GDL}^{\tau_{d,0}}}} \quad (12)$$

We would like to address that electrode thickness is not a fixed number; rather it varies from case to case, typically from 5 to 25 μm [25] [26]. In addition, porosity of GDL may vary from 0.6 to 0.8 as mentioned previously. Further, different cold-start strategies of current density may apply. Consequently, the Da number varies according to different combinations of physical and operating parameters.

It is of interest to evaluate the oxygen concentration drop across the catalyst layer, which is small (<0.5 mol/m^3) at 0.1 A/cm^2, $\tau_{d,0}=\tau_d$=1.5 and s_{ice} <98%. Therefore, the solution of Eq. (10) is valid at s_{ice} up to 98%. When s_{ice} reaches a level that causes serious starvation (therefore j_c is no longer uniform and the transient term cannot be neglected), the solution, Eq. (10), is therefore invalid. Once the oxygen profile is available, further substituting Eq. (10) into Eq. (1) and again assuming uniform reaction rate yield [1]:

$$\eta(s_{ice},x)=-\frac{RT}{\alpha_c F}\ln\left\{\frac{I\delta_{CL}C_{O2,ref}}{a_0 i_{0,c}^{ref}C_{cCL}^{O2}}\left[(1-s_{ice})^{\tau_a}\left(1-Da\frac{1-(\frac{x-x_{cCL}}{\delta_{CL}}+1)^2}{\varepsilon_{CL}^{\tau_d-\tau_{d,0}}(1-s_{ice})^{\tau_d}}\right)\right]^{-1}\right\} \tag{13}$$

Therefore, a dimensionless function can be defined as

$$\Pi(s_{ice},x)=\ln\left[(1-s_{ice})^{\tau_a}\left(1-Da\frac{1-(\frac{x-x_{cCL}}{\delta_{CL}}+1)^2}{\varepsilon_{CL}^{\tau_d-\tau_{d,0}}(1-s_{ice})^{\tau_d}}\right)\right] \tag{14}$$

It can be seen that impacts of solid water are solely contained in the function Π. The function Π consists of two parts: one is from the reduction of electrochemical active surface due to solid water coverage, and the other is oxygen starvation. Then Eq. (13) can be written as

$$\eta(s_{ice},x)=-\frac{RT}{\alpha_c F}\ln\left[\frac{I\delta_{CL}C^{O2,ref}}{a_0 i_{0,c}^{ref}C_{cCL}^{O2}}\right]+\frac{RT}{\alpha_c F}\Pi(s_{ice},x)=\eta_{c,o}+\Delta\eta_c \tag{15}$$

Where

$$\eta_{c,o}=-\frac{RT}{\alpha_c F}\ln\left[\frac{I\delta_{CL}C^{O2,ref}}{a_0 i_{0,c}^{ref}C_{cCL}^{O2}}\right]\ \text{and}\ \ \Delta\eta_c=\frac{RT}{\alpha_c F}\Pi(s_{ice},x) \tag{16}$$

$\eta_{c,o}$ denotes the overpotential at the interface between the cathode catalyst layer and GDL when no ice is present. The overpotential change due to ice presence can be further expressed as

$$\Delta\eta_c(s_{ice},x)=\Delta\eta_{c,1}+\Delta\eta_{c,2} \tag{17}$$

Where

$$\Delta\eta_{c,1}=\tau_a\frac{RT}{\alpha_c F}\ln(1-s_{ice})\ \text{and}\ \Delta\eta_{c,2}=\frac{RT}{\alpha_c F}\ln\left(1-Da\frac{1-(\frac{x-x_{cCL}}{\delta_{CL}}+1)^2}{\varepsilon_{CL}^{\tau_d-\tau_{d,0}}(1-s_{ice})^{\tau_d}}\right) \tag{18}$$

$\Delta\eta_{c,1}$ and $\Delta\eta_{c,2}$ represent the voltage losses due to the reactive surface reduction and oxygen starvation, respectively. Therefore, a dimensionless parameter β_3 can be defined as the ratio of these two

$$\beta_3 = \frac{\Delta\eta_{c,1}}{\Delta\eta_{c,2}} \tag{19}$$

Finally, the cell voltage can be calculated once the cathode overpotential is obtained:

$$V_{cell} = U_o + \eta_c - \eta_a - R_\Omega I \tag{20}$$

The last term on the right side represents the Ohmic loss, which usually consists of the ionic resistances in the membrane and catalyst layer and electronic components in circuit, as well as the potential contact resistance. Details of calculation can be found in Ref. 1.

RESULTS AND DISCUSSIONS

Table 1 Geometrical, physical and operating parameters

Quantity	**Value**
Catalyst layer/GDL/BP thickness $\delta_{CL}/\delta_{GDL}/\delta_{BP}$	0.0075-0.025/0.2/2-4 mm
Porosity of GDL/catalyst layers $\varepsilon_{GDL}/\varepsilon_{CL}$	0.5-0.8/0.3-0.8
Volume fraction of ionomer in the catalyst layer ε_m	0.13-0.40
Density of ice/dry membrane ρ_{ice}/ρ_m	917/1980 kg/m^3
O_2 diffusivity in cathode gas at standard condition	$3.24\times10^{-5} m^2/s$
Net water transport per proton, α	0.1
Electron transfer coefficient, α_c	0.5-1.0
Exchange current density × reaction surface area, $a_0 i_0$	10000.0 A/m^3

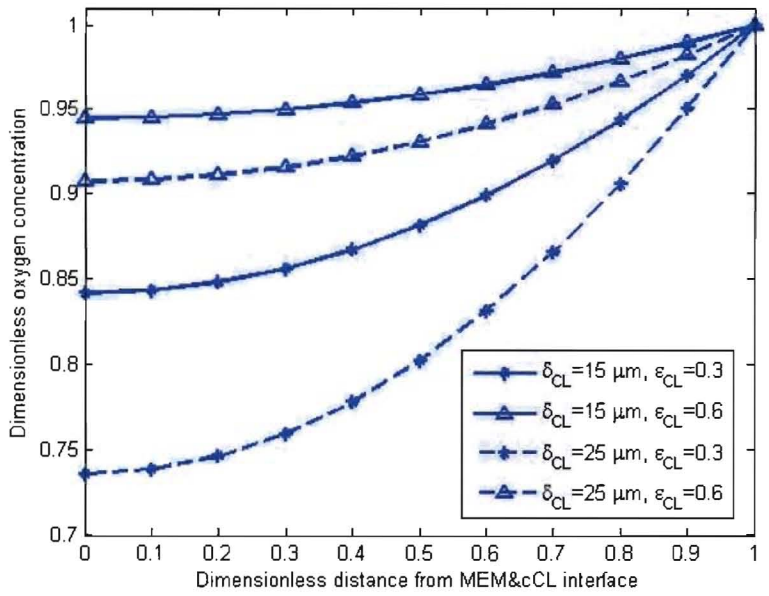

Fig. 3. Oxygen profiles in the cathode catalyst layer at different δ_{CL} s and ε_{CL} s at ice volume fraction of 0.98.

Figure 3 shows the oxygen profiles in the cathode catalyst layer, scaled by the O_2 concentration at the interface of cathode catalyst layer and GDL (i.e. x_{cCL}). At this stage of the ice volume fraction, the oxygen concentration may drop 25% when the electrode thickness of 25 μm is considered. For other thin electrodes or high porosity, small variations are observed. Therefore, the oxygen transport limitation takes place in a fairly latter part of the cold start (~ice volume fraction of 0.98).

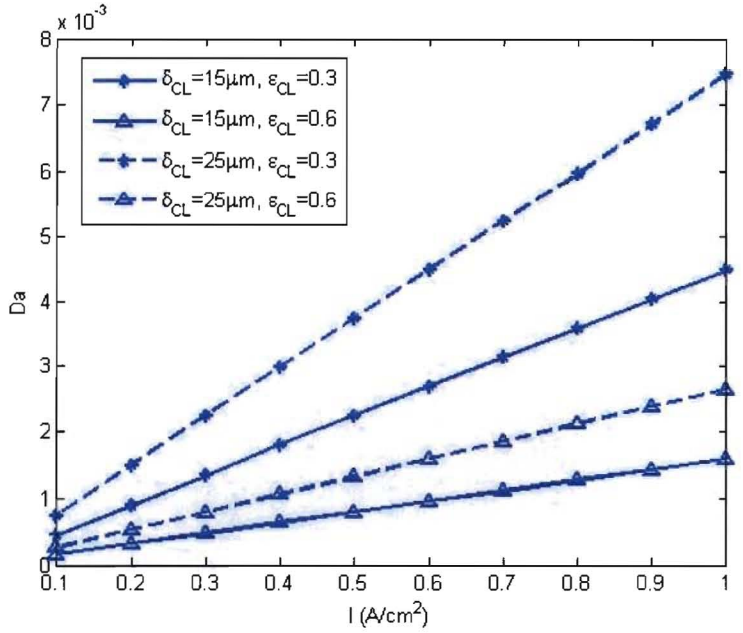

Fig. 4. Da number v.s. I for different catalyst layer thicknesses and porosities for tortuosity of 1.5.

Figure 4 plotted the important parameter Da number against I for different catalyst layer configurations. As reviewed previously, several typical thickness and porosity values are considered and show the range of Da is from 10^{-4} to 10^{-2}. The Da number compares reaction rate and mass transport rate, therefore the range shown in this figure indicates mass transport rate is much higher than the reaction rate in the catalyst layer when no ice presents. As solid water is added, the void space becomes smaller, leading to the increase of the mass transport limitation where the cell performance will respond with a fast drop. Note that in our definition, we excludes ice volume fraction in the Da number. A similar definition can be made to include it in the Da. In that case, the Da number will increase upon ice volume growth.

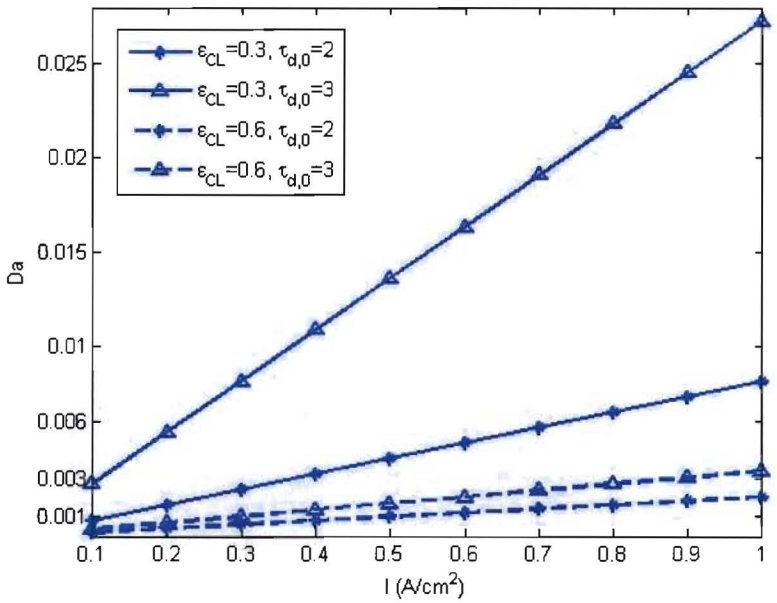

Fig. 5. Da number dependence of *I* for different porous medium tortuosity $\tau_{d,0}$ s and catalyst layer porosity ε_{CL} s.

As Da is an important parameter, we further plot it in Figure 5 for different $\tau_{d,0}$ s and ε_{CL} s given a fixed electrode thickness of 15 μm. Clearly, $\tau_{d,0}$ has profound impact on the cell performance: as the tortuosity increases from 2.0 to 3.0, the Da number jumps more than two times higher for lower porosity. It's also worthy to note that the tortuosity may be even higher as indicated by Ref. [18]. In addition, typically the current density at cold-start is low around 0.1 A/cm^2, which leads to much small Da, in the range of ~10^{-3}.

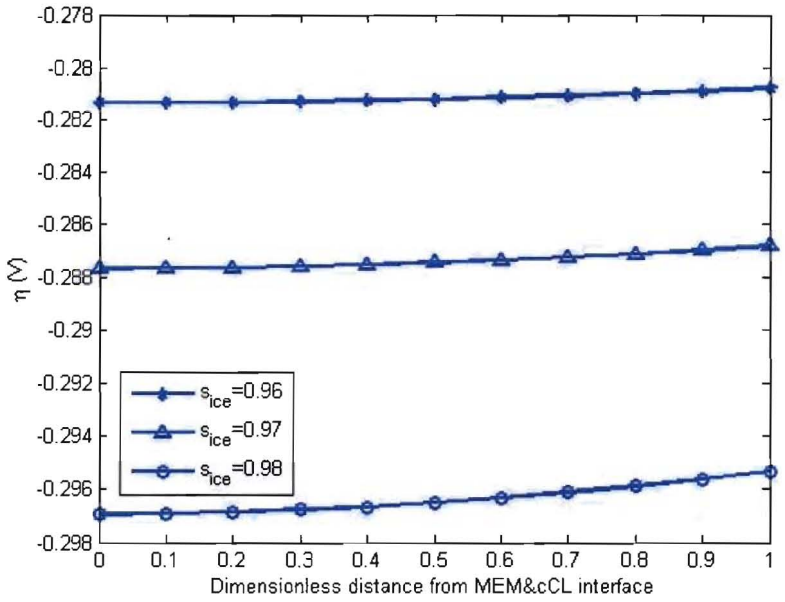

Fig. 6. η profiles in the cathode catalyst layer for different s_{ice} s at I of 0.1 A/cm^2, $C_{cCL}^{O_2}$ of 10 mol/m^3, T of -30 $^{\circ}C$, ε_{CL} of 0.5 and δ_{CL} of 15 μm.

The surface overpotential as a function of dimensionless distance is plotted in Figure 6. It is of interest that the overpotential is almost constant at different times (note that s_{ice} is a function of time). However, it decreases uniformly with time. This is due to the fact that solid water affects the local electrochemical activity, making surface overpotential decrease. Note that at the level of ice volume fraction considered, the oxygen transport limitation is not the dominant mechanism for cell voltage loss.

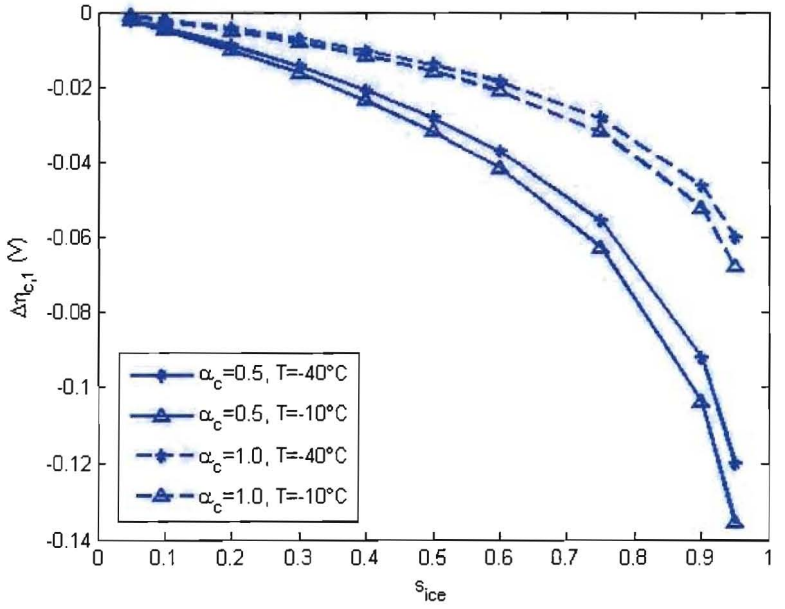

Fig. 7. $\Delta\eta_{c,1}$ dependence of s_{ice} at different electron transfer coefficient α_c and temperatures.

$\Delta\eta_{c,1}$ represents the voltage losses due to the reactive surface reduction arising from solid water coverage, which is plotted in Figure 7. Its magnitude increases at a fast pace with s_{ice}, therefore this mechanism becomes more important in latter stage of cold start. Also before s_{ice} reaches 50%, magnitude of $\Delta\eta_{c,1}$ is less than 0.03 V in all the range of α_c, indicating that voltage loss due to this mechanism is small in the initial stage. Even at 90%, the loss is less than 0.12 V.

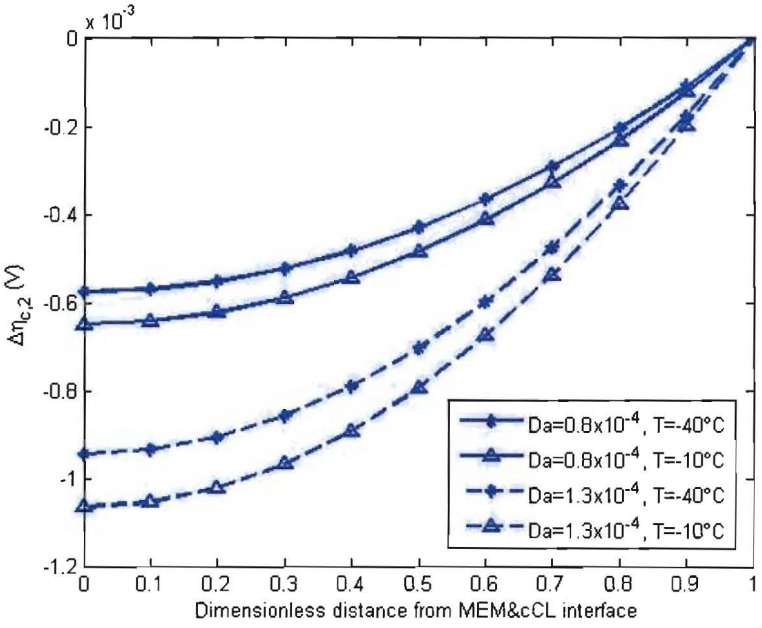

Fig. 8. $\Delta\eta_{c,2}$ profiles at different temperatures and Da numbers at s_{ice} of 0.98.

Figure 8 shows the profiles of $\Delta\eta_{c,2}$ across the cathode electrode. Even though variation is observed, the magnitude is actually fairly small in the scale of 1 mV. Not surprisingly, higher Da number corresponds to larger magnitude of $\Delta\eta_{c,2}$ that indicates the voltage loss due to oxygen concentration change. In addition, the analysis assumes a uniform current density within the catalyst layer during cold start, this "ideal" condition ensures simplified analysis that quantitative comparisons can be made to show the importance of solid water impact mechanisms through the variation of overpotential. In this figure, as the overpotential variation is small ~1 mV, therefore the oxygen transport limitation in the catalyst layer has not started yet at s_{ice}=0.98, which is consistent with our previous analysis.

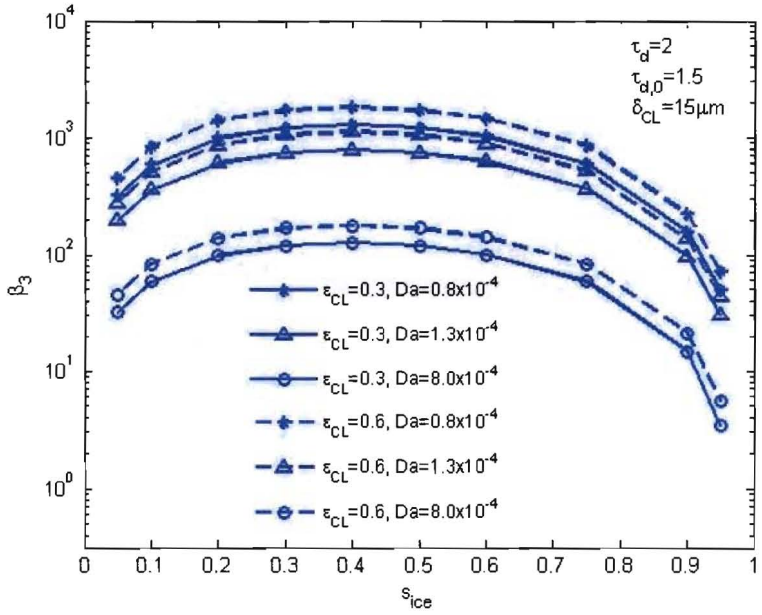

Fig. 9. β_3 dependence of s_{ice} at different catalyst layer porosity ε_{CL} s and Da numbers.

The dimensionless parameter β_3 is plotted in Figure 9, which is defined as the ratio of the two mechanisms of solid water impact on cell performance. It can be seen that the reaction surface reduction is more important than the one caused by oxygen transport limitation in the range considered. Its magnitude of importance, i.e. the ratio, increases with ice volume fraction at the initial stage, followed by a decrease but still in the range of 10-100 in most part. It is also worthy to note that the ratio may reach over 1000, indicating the importance of catalyst surface reduction by solid water during cold start. Of course, as ice volume fraction is further increases, the oxygen transport limitation will start to dominate. However, it is not plotted in the figure as the model is invalid during such a short period.

CONCLUSIONS

This paper investigated the electrochemical kinetics and oxygen transport within the cathode catalyst layer of a fuel cell during cold start. We simplified the model to link the mechanisms of solid water impacts on cell performance to the surface overpotential variation, which allows the explicitly decoupling of the two important mechanisms of ice effect, i.e. oxygen transport limitation and electrochemical catalyst surface reduction. Several key parameters of PEFC coldstart are defined and evaluated in the typical ranges of depending factors. It found that the Da number is generally small therefore mass transport limitation is not an issue within catalyst layer as long as ice volume fraction is not exceedingly high. In addition, comparison of the two mechanisms showed that the electrochemical catalyst surface reduction may play a much more important role during cell cold start.

Acknowledgments

Partial support of this work by the UC Irvine Academic Senate Council on Research, Computing and Library Resources (CORCLR) is gratefully acknowledged.

References

[1] Y. Wang, *J. Electrochem. Soc.*, **154**, B1041 (2007).
[2] J. Larminie and A. Dicks, *Fuel Cell Systems Explained*, 2nd ed., John Wiley & Sons, New York (2003).
[3] J. Amphlett, R. Mann, B. Peppley, P. Roberge and A. Rodrigues, *J. Power Sources* **61**, 183 (1996).
[4] Y. Wang and C.-Y. Wang, *Electrochim. Acta* **50**, 1307 (2005).
[5] Y. Wang and C.-Y. Wang, *Electrochim. Acta* **51**, 3924 (2006).
[6] Q. Yan, H. Toghiani and H. Causey, *J. Power Sources* **161**, 492 (2006).
[7] J. Chen and B. Zhou, *J. Power Sources* **177**, 83 (2008).
[8] C. Y. Wang, *Chem. Rev.*, **104**, 4727 (2004).
[9] L. Mao, C.Y. Wang and Y. Tabuchi, *J. Electrochem. Soc.*, **154**, B341 (2007).
[10] H. Meng, *J. Power Sources*, **178,** 141 (2008).
[11] A. Parthasarathy, S. Srinivasan and A. J. Appleby, *J. Electrochem. Soc.*, **139**, 2530 (1992).
[12] J. Zhang, Y. Tang, C. Song, J. Zhang and H. Wang, *J. Power Sources* **163**, 532 (2006).
[13] T. Springer, T. Zawodzinski and S. Gottesfeld, *J. Electrochem. Soc.*, **138**, 2334 (1991).
[14] Y. Wang, C.-Y. Wang, *J. Power Sources* **147**, 148 (2005).
[15] A. D. Le and B. Zhou, *J. Power Sources* **182**, 197 (2008).
[16] H. Sun, H. Liu and L. Guo, *J. Power Sources* **143**, 125 (2005).
[17] Y. Wang, C.-Y. Wang and K. S. Chen, *Electrochim. Acta*, **52**, 3965 (2007).
[18] P. Mukherjee and C.-Y. Wang, *J. Electrochem. Soc.*, **153**, A840 (2006).
[19] E. Kumbur, K. Sharp, and M. Mench, *J. Electrochem. Soc.*,**154**, B1305 (2007).
[20] E. Kumbur, K. Sharp, and M. Mench, *J. Electrochem. Soc.*,**154**, B1315 (2007).
[21] U. Pasaogullari, C.-Y. Wang, and K. S. Chen, *J. Electrochem. Soc.*, **152**, A1574 (2005).
[22] H. Lin, C. Cheng, C. Soong, F. Chen and W. Yan, *J. Power Sources* **162**, 246 (2006).
[23] M. Han, J. H. Xu, S. H. Shan and S. P. Jiang, *Electrochim. Acta*, **53**, 5361 (2008).
[24] I. Nitta, T. Hottinen, O. Himanena and M. Mikkola, *J. Power Sources* **171**, 26 (2007).
[25] E.Thompson, J. Jorne, W. Gu and H. Gasteiger, *J. Electrochem. Soc.*, **155**, B625 (2008).
[26] A. Haug, R. White, J. Weidner, W. Huang, S. Shi, T. Stoner and N. Rana, *J. Electrochem. Soc.*, **149**, A280 (2002).